

**High affinity interactions of Pb<sup>2+</sup> with Synaptotagmin I**

Journal:	<i>Metallomics</i>
Manuscript ID	MT-ART-06-2018-000135.R1
Article Type:	Paper
Date Submitted by the Author:	16-Jul-2018
Complete List of Authors:	Katti, Sachin; Texas A&M University, Biochemistry and Biophysics Her, Bin; Texas A&M University, Biochemistry and Biophysics Srivastava, Atul; Texas A&M University, Biochemistry and Biophysics Taylor, Alexander; University of Texas Health Science Center at San Antonio, Department of Biochemistry and Structural Biology lockless, Steve; Texas A&M University, Biology Igumenova, Tatyana; Texas A&M University, Biochemistry and Biophysics

## High affinity interactions of Pb<sup>2+</sup> with Synaptotagmin I

Sachin Katti,<sup>1</sup> Bin Her,<sup>1</sup> Atul K. Srivastava,<sup>1</sup> Alexander B. Taylor,<sup>2</sup> Steve W. Lockless,<sup>3</sup> and  
Tatyana I. Igumenova<sup>1,\*</sup>

<sup>1</sup>Department of Biochemistry and Biophysics, Texas A&M University, 300 Olsen Boulevard,  
College Station, TX 77843, United States

<sup>2</sup>Department of Biochemistry and Structural Biology and the X-ray Crystallography Core  
Laboratory, Institutional Research Cores, University of Texas Health Science Center at San  
Antonio, San Antonio, TX 78229, United States

<sup>3</sup>Department of Biology, Texas A&M University, 3258 TAMU, TX 77843, United States

**ABSTRACT** [163 words]

Lead (Pb) is a potent neurotoxin that disrupts synaptic neurotransmission. We report that Synaptotagmin I (SytI), a key regulator of  $\text{Ca}^{2+}$ -evoked neurotransmitter release, has two high-affinity  $\text{Pb}^{2+}$  binding sites that belong to its cytosolic C2A and C2B domains. The crystal structures of  $\text{Pb}^{2+}$ -complexed C2 domains revealed that protein-bound  $\text{Pb}^{2+}$  ions have holodirected coordination geometries and all-oxygen coordination spheres. The on-rate constants of  $\text{Pb}^{2+}$  binding to the C2 domains of SytI are comparable to those of  $\text{Ca}^{2+}$  and are diffusion-limited. In contrast, the off-rate constants are at least two orders of magnitude smaller, indicating that  $\text{Pb}^{2+}$  can serve as both thermodynamic and kinetic trap for the C2 domains. We demonstrate, using NMR spectroscopy, that population of these sites by  $\text{Pb}^{2+}$  ions inhibits further  $\text{Ca}^{2+}$  binding despite the existing coordination vacancies. Our work offers a unique insight into the bioinorganic chemistry of Pb(II) and suggests a mechanism by which low concentrations of  $\text{Pb}^{2+}$  ions can interfere with the  $\text{Ca}^{2+}$ -dependent function of SytI in the cell.

**Significance to Metalloomics**

Several signaling proteins that were identified as molecular targets of  $\text{Pb}^{2+}$  contain C2 domains. C2 domains are  $\text{Ca}^{2+}$ -dependent peripheral membrane modules that specifically bind to anionic phospholipids. We demonstrate that  $\text{Pb}^{2+}$  successfully targets oxygen-rich  $\text{Ca}^{2+}$  coordination sites of both C2 domains in SytI, a key regulator of neurotransmitter release. Our data provide structural and mechanistic insights into potential modes of  $\text{Pb}^{2+}$  toxicity and interference with  $\text{Ca}^{2+}$ -regulated processes.

## INTRODUCTION

Lead poisoning remains a pervasive public health problem, as illustrated by the recent outbreaks in the U.S. (Flint, Michigan) and abroad.<sup>1,2</sup> Lead exposure is especially detrimental in young children, resulting in serious neurodevelopmental and psychological disorders.<sup>3-5</sup> The potency of  $\text{Pb}^{2+}$  ( $[\text{Xe}]4f^{14}5d^{10}6s^2$ ) stems from its ability to cross the blood-brain barrier<sup>6</sup> and preferentially target  $\text{Zn}^{2+}$  and  $\text{Ca}^{2+}$  coordination sites of biological macromolecules.<sup>7-9</sup> The ability of  $\text{Pb}^{2+}$  to mimic these essential divalent metal ions results in disruption of cellular signaling, ion transport, and calcium homeostasis.<sup>10-13</sup>

The molecular mechanisms of  $\text{Pb}^{2+}$  neurotoxicity are not well understood. Several neuronal proteins associated with  $\text{Ca}^{2+}$  signaling have been implicated in  $\text{Pb}^{2+}$  toxicity (reviewed in<sup>8</sup>). Among them are the voltage-gated  $\text{Ca}^{2+}$  channels, where the putative mechanism is the blockage of  $\text{Ca}^{2+}$  currents due to  $\text{Pb}^{2+}$  interactions with ion selectivity filters.<sup>14, 15</sup> Another example is the ligand-gated ionotropic N-methyl D-aspartate receptor (NMDAR),<sup>16, 17</sup> where  $\text{Pb}^{2+}$  acts as an antagonist, partly through the interactions with the allosteric  $\text{Zn}^{2+}$  regulatory site<sup>18</sup> in the extracellular domain of the receptor. An important class of  $\text{Pb}^{2+}$  targets are the intracellular  $\text{Ca}^{2+}$ -sensor proteins, such as Synaptotagmin I (SytI),<sup>19</sup> Calmodulin (CaM),<sup>20, 21</sup> and protein kinase C (PKC).<sup>22, 23</sup>

While the proteins in question are quite distinct in their structure and function, one shared feature is the prevalence of oxygen donor ligands in their metal-ion coordination sites. The proposed NMDAR  $\text{Pb}^{2+}$ -binding site comprises the oxygens of aspartate and glutamate carboxylate groups, along with additional nitrogen ligands provided by histidine residues.<sup>24</sup> The selectivity filters of  $\text{Ca}^{2+}$  channels,<sup>14, 25</sup> the EF hand motif of CaM,<sup>21</sup> and the loop regions of the  $\text{Ca}^{2+}$ -dependent phospholipid-binding conserved homology 2 (C2) domains of SytI<sup>19, 26</sup> and

1  
2  
3 PKC<sup>23</sup> have all-oxygen metal-ion coordination sites capable of interactions with Pb<sup>2+</sup>. The  
4  
5 analysis of Pb<sup>2+</sup>-bound protein structures in the PDB revealed that about 79% of the Pb<sup>2+</sup>-  
6  
7 coordinating ligands are oxygen atoms that belong to the sidechain carboxylate and backbone  
8  
9 carbonyl moieties of proteins, in addition to surrounding water molecules.<sup>27</sup> The objective of  
10  
11 this work was to determine what makes Pb<sup>2+</sup> an effective competitor for oxygen-rich  
12  
13 coordination sites in proteins, using SytI as a paradigm.  
14  
15

16  
17 SytI is an integral membrane protein that serves as a Ca<sup>2+</sup>-dependent trigger of synchronous  
18  
19 neurotransmitter release.<sup>28</sup> The N-terminal segment of SytI is a transmembrane helical domain  
20  
21 that anchors the protein to synaptic vesicle (**Fig. 1a**). The cytosolic C-terminal region comprises  
22  
23 two Ca<sup>2+</sup>-sensing C2 domains, C2A and C2B. These domains have tri-partite (C2A) and bi-  
24  
25 partite (C2B) Ca<sup>2+</sup> binding motifs that are believed to be targeted by Pb<sup>2+</sup> with unknown  
26  
27 stoichiometry.<sup>19, 26</sup> The intrinsic Ca<sup>2+</sup> affinities are pH-dependent and weak, ranging from 50  
28  
29  $\mu\text{M}$  to >10 mM.<sup>29-31</sup> Ca<sup>2+</sup> binding generates a localized electropositive potential in the apical C2  
30  
31 loop region and thereby enables SytI to interact with presynaptic membranes and SNARE  
32  
33 proteins (**Fig. 1a**).<sup>29, 32-36</sup> The outcome is the exocytic membrane fusion with the concomitant  
34  
35 release of neurotransmitters into the synaptic cleft.  
36  
37  
38  
39

40  
41 In this work, we demonstrate that SytI has two high-affinity Pb<sup>2+</sup> binding sites, one per C2  
42  
43 domain. These high-affinity interactions, combined with fast binding and slow dissociation,  
44  
45 impart thermodynamic and kinetic advantage on Pb<sup>2+</sup> compared to Ca<sup>2+</sup>. Moreover, a single Pb<sup>2+</sup>  
46  
47 ion binding to either C2 domain has a profound inhibitory effect on subsequent Ca<sup>2+</sup> binding,  
48  
49 despite the existing coordination vacancies. Together, the inhibition of Ca<sup>2+</sup> binding and  
50  
51 previously known ability of Pb<sup>2+</sup> to trigger membrane association of C2 domains<sup>19, 23, 37</sup> provide  
52  
53 a potential mechanism to explain the effect of Pb<sup>2+</sup> on neurotransmitter release.  
54  
55  
56  
57  
58  
59  
60

## METHODS

### *Materials*

The working solutions of metal ions were prepared in HPLC grade water or decalcified buffers using the following salts: Pb(II) acetate tri-hydrate (Sigma-Aldrich), standardized 1 M solution of Ca(II) chloride (Fluka Analytical), and Tb(III) chloride hexahydrate (Acros Organics). Prior to use, all buffers were treated with the ion-chelating resin Chelex 100 (Sigma-Aldrich) to remove trace divalent metals. Lipid components used in the phospholipid vesicle preparations: 1-palmitoyl-2-oleoyl-sn-glycero-3-phosphocholine (POPC) and 1-palmitoyl-2-oleoyl-sn-glycero-3-phospho-L-serine (POPS) were obtained from Avanti Polar Lipids Inc. (Alabaster, AL). The quartz cuvettes used for the Tb<sup>3+</sup> luminescence experiments were coated with Sigmacote® to avoid the protein adhesion to the walls. The cDNA of murine Syt1 was purchased from Open Biosystems (GE Life Sciences). All protein constructs were expressed and purified as described in the SI.

### *Crystallization, structure determination and refinement*

The samples used for crystallization of SytI domains with Pb<sup>2+</sup> contained: (i) 17 mg/mL C2A with 7 mM Pb(II) acetate, and (ii) 22 mg/mL C2B with 1.1 mM Pb(II) acetate in 20 mM MES buffer at pH 6.0. Screening for crystallization was carried out in automated manner by using the sitting drop vapor-diffusion method with an Art Robbins Instruments Phoenix system in the X-ray Crystallography Core Laboratory at UTHSCSA. Crystals for Pb<sup>2+</sup>-bound C2A were obtained from Qiagen Classics II Suite condition #74 (0.2 M lithium sulfate, 0.1 M bis-tris pH 5.5, 25% polyethylene glycol 3350) at 4 °C. Although C2B was loaded with Pb<sup>2+</sup> prior to crystallization, it was difficult to produce a Pb<sup>2+</sup>-loaded C2B crystal as the metal was typically lost resulting in

1  
2  
3 apo-C2B crystals. Crystals for  $\text{Pb}^{2+}$ -bound C2B were ultimately obtained from Microlytic  
4 MCSG-2 Suite condition #33 (0.2 M sodium fluoride, 20% polyethylene glycol 3350) at 22 °C.  
5  
6 The crystals exhibited low occupancy  $\text{Pb}^{2+}$ -binding during refinement of the structure  
7  
8 coordinates, so an additional crystal was soaked overnight in mother liquor containing 5 mM  
9  
10 lead acetate. This technique was applied to promote complete  $\text{Pb}^{2+}$ -binding since the unsoaked  
11  
12 crystal structure showed ambiguity in some of the electron density containing the binding site.  
13  
14 The details of structure determination and refinement are given in the SI, along with the data  
15  
16 collection and refinement statistics (**Table S1**). The refined coordinates of the  $\text{Pb}^{2+}$  complexes  
17  
18 of C2A and C2B were deposited in the Protein Data Bank under accession codes 5vfe and 5vfg  
19  
20 (5vff for partial  $\text{Pb}^{2+}$  occupancy), respectively. The analysis of metal-oxygen distances and the  
21  
22 calculation of backbone r.m.s.d. from the previously published SytI structures (**Tables S2-S5**)  
23  
24 was conducted using UCSF Chimera.<sup>38</sup>  
25  
26  
27  
28  
29  
30  
31  
32

### 33 *Isothermal Titration Calorimetry (ITC)*

34  
35 For ITC experiments, the C2A and C2B domains of SytI were extensively dialyzed against  
36  
37 the large excess of decalcified ITC buffer (20 mM MES at pH 6.0 with 150 mM KCl). The  
38  
39 filtered and degassed dialysis buffer was then used to prepare 50  $\mu\text{M}$  C2A/C2B and 0.5 mM  $\text{Pb}^{2+}$   
40  
41 working solutions. The measurements for the heat of binding were carried out in MicroCal  
42  
43 iTC200 (Malvern Panalytical) instrument with 14 successive additions of  $\text{Pb}^{2+}$  stock solution (0.5  
44  
45  $\mu\text{l}$  for the first injection and 3  $\mu\text{l}$  for all subsequent injections) into the protein. The acquisition  
46  
47 and analysis of the triplicates was done using Origin software; the data were fit into a single set-  
48  
49 of-sites binding model.  
50  
51  
52  
53  
54  
55  
56  
57  
58  
59  
60

## ***Nuclear Magnetic Resonance (NMR) spectroscopy***

### *NMR-detected Pb<sup>2+</sup> binding to C2 domains*

NMR-detected Pb<sup>2+</sup> binding to [U-<sup>15</sup>N] enriched SytI C2 domains was monitored by acquiring series of <sup>1</sup>H-<sup>15</sup>N HSQC spectra at 25 °C on Bruker AVANCE III spectrometers operating at <sup>1</sup>H Larmor frequencies of 500 MHz (C2B) and 600 MHz (C2A). Protein concentration of 100 μM in decalcified 20 mM MES buffer (pH 6.0), 0.02% NaN<sub>3</sub>, and 8% D<sub>2</sub>O was used for all binding experiments. The Pb<sup>2+</sup> concentrations were: 0, 0.025, 0.05, 0.075, 0.1, 0.125, 0.15, 0.2, 0.3, 0.4, 0.5, 0.75, 1.0, 1.3, 1.6, 2.0, and 2.5 mM for C2A; and 0, 0.0125, 0.025, 0.05, 0.075, 0.1, 0.125, 0.15, 0.2, 0.25, 0.3, 0.4, 0.5, 0.6, 0.8, 1.5, and 3.0 mM for C2B. The spectra were processed using NMRPipe<sup>39</sup> and analyzed using Sparky.<sup>40</sup> The chemical shift perturbation (CSP) due to M<sup>2+</sup> binding, Δ, was calculated using the following equation:

$$\Delta = [\Delta\delta_H^2 + (0.152\Delta\delta_N)^2]^{1/2} \quad (1)$$

where Δδ<sub>H</sub> and Δδ<sub>N</sub> are residue-specific <sup>1</sup>H and <sup>15</sup>N chemical shift differences between the apo and Pb<sup>2+</sup> bound states of the proteins. Pb<sup>2+</sup> binding curves for the second site of the respective domains were constructed by plotting Δ as a function of corrected Pb<sup>2+</sup> concentration to take into account the partial occupancy of the first metal binding sites. The binding curves were globally fitted (12 C2A, and 9 C2B residues) with a single-site binding model:

$$\Delta = (\Delta_{max} / 2P_0) [(K_d + P_0 + L_0) - ((K_d + P_0 + L_0)^2 - 4P_0L_0)^{1/2}] \quad (2)$$

where Δ is the CSP value between the apo and Pb<sup>2+</sup>-bound state; Δ<sub>max</sub> is the maximum CSP value reached upon Site 2 saturation; and P<sub>0</sub> and L<sub>0</sub> are the total protein and Pb<sup>2+</sup> concentrations, the latter corrected for Pb<sup>2+</sup> populating Site 1.

### *ZZ exchange NMR spectroscopy*



1  
2  
3 The kinetic parameters of  $\text{Pb}^{2+}$  binding to the high-affinity sites of  $[\text{U-}^{15}\text{N}]$  enriched SytI C2  
4 domains were obtained by acquiring a series of ZZ exchange experiments<sup>41</sup> on the cryoprobe-  
5 equipped Bruker AVANCE III spectrometers operating at  $^1\text{H}$  Larmor frequencies of 800 MHz  
6 (C2A) and 600 MHz (C2B). The data were collected at 4 different temperatures: 10, 15, 20, and  
7 25 °C. The temperatures were calibrated using deuterated methanol. The protein samples (350  
8  $\mu\text{M}$ ) were prepared in decalcified 20 mM MES buffer (pH 6.0), 150 mM KCl, 0.02%  $\text{NaN}_3$ , and  
9 8%  $\text{D}_2\text{O}$ .  $\text{Pb}^{2+}$  was added to a concentration of 175  $\mu\text{M}$  to generate approximately equal  
10 populations of the apo- and  $\text{Pb}^{2+}$ -bound proteins. The samples were equilibrated overnight. The  
11 exchange between the two states, apo and  $\text{Pb}^{2+}$ -bound, resulted in the transfer of longitudinal  $^{15}\text{N}$   
12 magnetization during the variable mixing time period, manifested as the build-up of the cross-  
13 peak intensities and decay of the auto-peak intensities. The respective build-up and decay of the  
14 cross-peak and auto-peak intensities for the well-resolved residues was quantified as a function  
15 of effective mixing times: 12.53, 17.53, 22.53, 27.53, 32.53, 37.53, and 42.53 ms for C2A and an  
16 additional point of 52.53 ms for C2B (**Fig. S3**). Effective mixing times,  $t_{\text{mix}}$ , were calculated as  
17 the duration of the mixing period plus 12.53 ms, which the time that  $^{15}\text{N}$  magnetization was  
18 longitudinal during the other elements of the pulse sequence. The spectra were processed using  
19 NMRPipe<sup>39</sup> and analyzed using Sparky.<sup>40</sup> The analysis of the ZZ exchange data was conducted  
20 as described in the SI, following the formalism of Miloushev et al.<sup>42</sup>  
21  
22  
23  
24  
25  
26  
27  
28  
29  
30  
31  
32  
33  
34  
35  
36  
37  
38  
39  
40  
41  
42  
43  
44  
45  
46

#### 47 *Detection of mixed $\text{Pb}^{2+}/\text{Ca}^{2+}$ C2 species*

48  
49 The formation of  $\text{C2}\cdot\text{Pb}_1\cdot(\text{Ca})_n$  complexes ( $n=1,2$  for C2A and  $n=1$  for C2B) was monitored  
50 at 25 °C on Bruker AVANCE III spectrometers operating at  $^1\text{H}$  Larmor frequencies of 800 MHz  
51 (C2A) and 500 MHz (C2B). The C2 domains were first equilibrated with concentrations of  $\text{Pb}^{2+}$   
52  
53  
54  
55  
56  
57  
58  
59  
60

1  
2  
3 sufficient to selectively populate first metal binding sites in a buffer solution composed of  
4  
5 decalcified 20 mM MES (pH 6.0), 150 mM KCl, 0.02% NaN<sub>3</sub>, and 8% D<sub>2</sub>O. The aliquots of  
6  
7 Ca<sup>2+</sup> solution prepared in the NMR buffer were added to the samples to achieve concentrations  
8  
9 ranging from 100 μM to 40 mM. The spectral changes were monitored using <sup>15</sup>N-<sup>1</sup>H HSQC  
10  
11  
12 spectra.  
13  
14  
15  
16

17 *Tb<sup>3+</sup> luminescence and vesicle co-sedimentation experiments are described in the SI.*  
18  
19  
20  
21  
22  
23  
24  
25  
26  
27  
28  
29  
30  
31  
32  
33  
34  
35  
36  
37  
38  
39  
40  
41  
42  
43  
44  
45  
46  
47  
48  
49  
50  
51  
52  
53  
54  
55  
56  
57  
58  
59  
60

## RESULTS AND DISCUSSION

### **Pb<sup>2+</sup> targets Ca<sup>2+</sup> Site 1 in both C2 domains of SytI**

Previous studies of SytI suggested that Pb<sup>2+</sup> binding site resides on the C2A domain.<sup>19</sup> It was unclear to us from the structural viewpoint why C2A would be a preferred interaction site over C2B. To understand the structural basis of C2-Pb<sup>2+</sup> interactions in SytI, we determined two high-resolution crystal structures of Pb<sup>2+</sup>-complexed C2A and C2B domains. Both structures revealed the presence of a single Pb<sup>2+</sup> ion that was refined at high occupancy: C2A·Pb1 (1.4 Å, 5vfe) and C2B·Pb1 (1.8 Å, 5vfg) (**Table S1** and **Fig. 1b**). We found that the position of bound Pb<sup>2+</sup> ion (Pb1) coincides with that of the first Ca<sup>2+</sup> ion (subsequently referred to as Ca1, see **Fig. 1e,f**), as defined in previous structural studies of Ca<sup>2+</sup>-complexed C2 domains. Comparison of Pb<sup>2+</sup>-bound and apo structures showed that the most conformational changes due to Pb<sup>2+</sup>-binding are in the apical loop regions, specifically loop 1 in C2A and loop 3 in C2B (**Fig. 1b**). Close inspection of the Pb<sup>2+</sup> coordination sites revealed that these differences are due to the rotation of the coordinating aspartic acid sidechains towards the metal ion: Asp178 in C2A, and Asp365 and Asp303 in C2B (**Figs. 1c,d**). The conformational changes in the other regions of C2 domains are minor, as evidenced by the low r.m.s.d. values obtained from the comparative analysis of existing C2A and C2B structures (**Tables S2-S3**).

Pb<sup>2+</sup> ions bound to the C2A and C2B domains have a coordination number (CN) of 8. All ligands are oxygen atoms donated by the aspartic acid sidechains, one backbone carbonyl group, and one (or two in case of C2A) water molecules (**Figs. 1c,d**). The ligands are distributed uniformly in the coordination sphere, indicating that the 6s<sup>2</sup> lone pair of Pb<sup>2+</sup> is stereochemically inactive. The distribution of Pb-oxygen bond distances is narrow, ranging from 2.4 to 2.8 Å (**Tables S4-S5**). In coordination chemistry of Pb<sup>2+</sup>, uniform distribution of ligands and

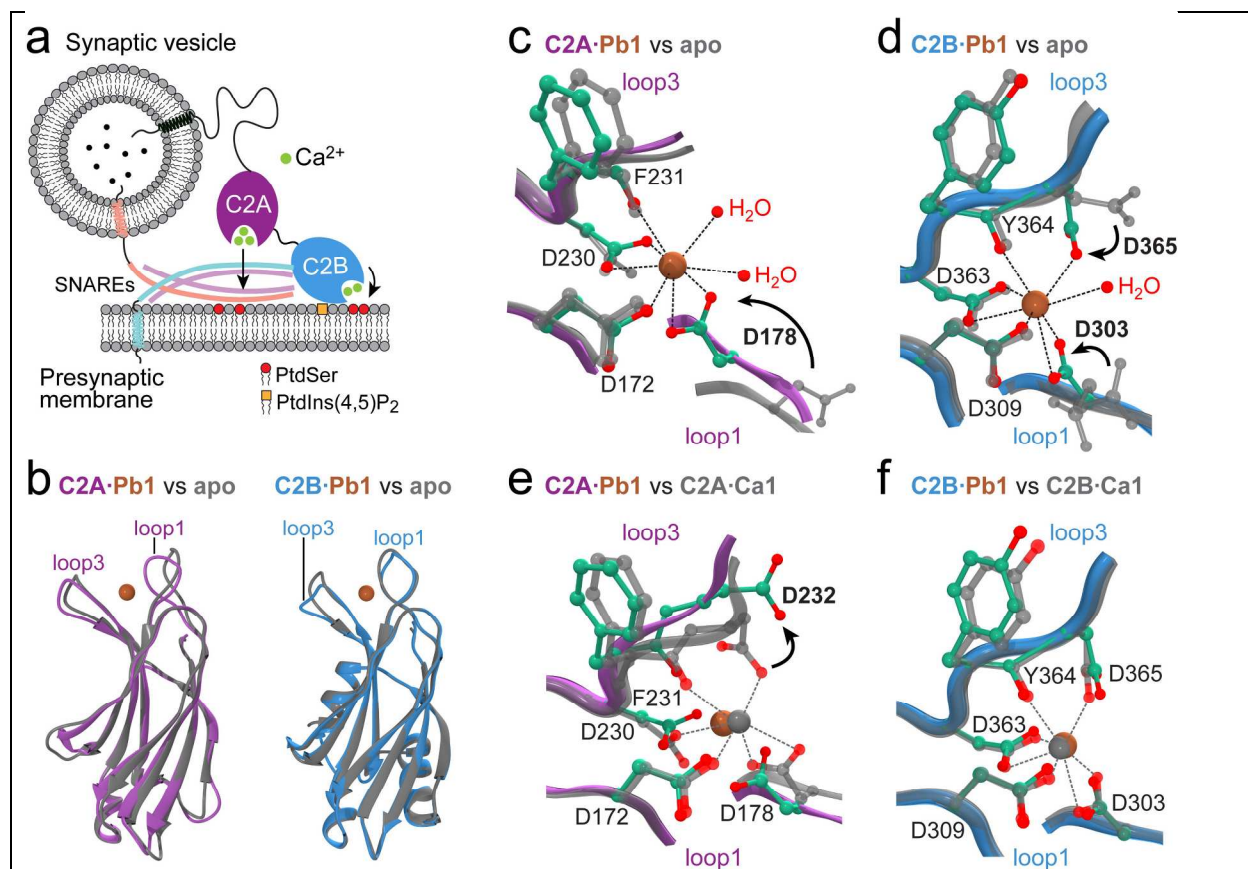


**Figure 1. Structural analysis of Pb<sup>2+</sup>-SytI interactions.** (a) SytI is a Ca<sup>2+</sup>-dependent trigger of exocytic membrane fusion. Ca<sup>2+</sup> binding to C2A and C2B domains drives their interaction with anionic phospholipids of the presynaptic membrane, PtdSer and PtdIns(4,5)P<sub>2</sub>. (b) Crystal structures of Pb<sup>2+</sup>-complexed C2 domains reveal a single bound Pb<sup>2+</sup> ion (sienna). Backbone superposition of Pb<sup>2+</sup>-complexed (C2A, purple and C2B, blue) and apo C2 domains (gray) illustrates the extent of conformational changes in the backbone of loop regions. The PDB identifiers are: 5vfe (C2A·Pb1), 4wee (apo C2A), 5vfg (C2B·Pb1), and 5ccj (apo C2B). (c,d) Octa-coordinated geometry of C2-bound Pb<sup>2+</sup>. The sidechain carbons and coordinating oxygens in the Pb<sup>2+</sup>-complexed structures are shown in green and red, respectively. All ligands are oxygen atoms donated by protein and water. Pb<sup>2+</sup> binding is accompanied by the conformational rearrangement of several coordinating residues that are shown in boldface. (e,f) Comparison of metal-ion coordination sites in Pb<sup>2+</sup>- and Ca<sup>2+</sup>-complexed C2A (1byn/NMR) and C2B (1tjx) domains. Pb<sup>2+</sup> and Ca<sup>2+</sup> are represented with sienna and gray spheres, respectively. The coordination geometry of Ca<sup>2+</sup> is shown with dashed lines. Only Ca1 and protein ligands are shown for clarity.

narrow range of Pb-ligand distances define a holodirected coordination geometry, which is favored in Pb<sup>2+</sup> sites with high CN values and bulky ligands.<sup>43</sup>

One notable difference between the Pb<sup>2+</sup>- and Ca<sup>2+</sup>-complexed C2A structures is a lack of coordination bond between Pb1 and the sidechain oxygens of Asp232, which points away from the metal ion binding site (**Fig. 1e**); in contrast, the Ca<sup>2+</sup>-Asp232 Oδ1 coordination bond is

1  
2  
3 present in the NMR structure of C2A (1byn).<sup>44</sup> In C2B, the coordination geometry of Ca1 and  
4  
5 Pb1 is identical, which is also reflected in the similarity of the backbone conformation of the  
6  
7 loop regions.  
8  
9

### 12 **Each C2 domain has one tight and one weak Pb<sup>2+</sup> site**

14 C2A and C2B have tri- and bi-partite Ca<sup>2+</sup>-binding motifs, respectively. To determine how  
15 many sites Pb<sup>2+</sup> populates in solution, we conducted NMR-detected binding experiments of Pb<sup>2+</sup>  
16  
17 to the C2 domains. The chemical shift changes of the N-H<sub>N</sub> backbone groups proximal to the  
18  
19 M<sup>2+</sup> coordination centers revealed two distinct Pb<sup>2+</sup> binding events in C2A (**Fig. 2a**) and C2B  
20  
21 (**Fig. 3a**). The first Pb<sup>2+</sup> binding event, which is “slow” on the NMR chemical shift timescale for  
22  
23 the majority of residues and saturates at approximately stoichiometric concentrations of Pb<sup>2+</sup>,  
24  
25 gives rise to two sets of cross-peaks that correspond to the apo C2 and the C2·Pb1 complex. The  
26  
27 second binding event is “fast”, manifesting itself in the smooth cross-peak trajectories as a  
28  
29 function of increasing total Pb<sup>2+</sup> concentration. These data indicate the presence of two Pb<sup>2+</sup>  
30  
31 sites with distinct kinetics and thermodynamics of binding. We did not observe an appreciable  
32  
33 population of Site 3 by Pb<sup>2+</sup> in the C2A domain.  
34  
35  
36  
37  
38  
39

40 To determine the influence of Pb<sup>2+</sup> binding on the C2 loop regions, we constructed the  
41  
42 chemical shift perturbation (CSP) plots for the high and low Pb<sup>2+</sup> concentration regimes (**Fig. 2b**  
43  
44 and **Fig. S1b**). The low concentration regime mostly reflects protein response to binding event  
45  
46 1, while the high concentration regime reflects the response to binding event 2. The CSP plot of  
47  
48 C2B shows that all three loop regions are affected by interactions with Pb<sup>2+</sup>, with the most  
49  
50 changes caused by the first binding event (**Fig. S1b**). In C2A, the second binding event  
51  
52 influences the residues of loop 3 more than those of loop 1 (**Fig. 2b**). Using this information in  
53  
54  
55  
56  
57  
58  
59  
60

conjunction with the  $\text{Ca}^{2+}$ -bound C2A structure, we can then assign the low-affinity  $\text{Pb}^{2+}$  site to Site 2 and high-affinity  $\text{Pb}^{2+}$  site to Site 1 in C2A, which is populated in the crystal structure of the  $\text{Pb}^{2+}$  complex.

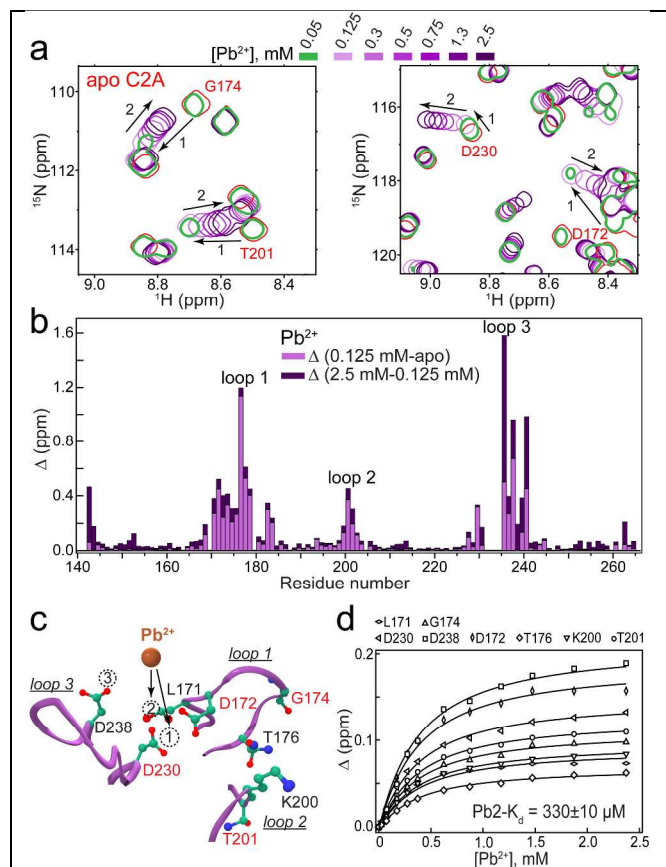


**Figure 2. C2A domain binds two  $\text{Pb}^{2+}$  ions in solution.** (a) Expansions of the C2A  $^{15}\text{N}$ - $^1\text{H}$  HSQC region for  $\text{Pb}^{2+}$  concentrations ranging from 0 to 2.5 mM. Peak displacements due to binding  $\text{Pb}1$  (1, slow exchange) and  $\text{Pb}2$  (2, fast exchange) are shown with arrows. (b) C2A chemical shift perturbation plot constructed for the low- ( $< 0.125$  mM) and high- ( $> 0.125$  mM) concentration regimes of  $\text{Pb}^{2+}$ . (c) Loop region of the C2A showing the location of  $\text{Ca}^{2+}$  sites 1-3, along with residues whose  $^{15}\text{N}$ - $^1\text{H}$  cross-peaks are labelled in (a) and/or used in (d). (d) NMR-detected binding curves constructed for the low-affinity  $\text{Pb}^{2+}$  Site 2. Solid lines represent the global fit that produced the  $K_d$  of  $330 \pm 10 \mu\text{M}$ .

We used the fast-exchange NMR data to construct the binding curves and obtain  $Pb^{2+}$  affinities to Site 2 of the C2 domains (see **Fig. 2c** and **Fig. 3b** for the Site 2 location). Global fitting of the binding curves produced  $K_d$  values of  $330 \pm 10 \mu M$  (C2A, **Fig. 2d**) and  $220 \pm 5 \mu M$  (C2B, **Fig. S1c**). The  $Ca^{2+}$  affinities for the same sites under identical buffer conditions are 1.6 mM (C2A) and 0.7-0.8 mM (C2B).<sup>31</sup> This means that the affinity of  $Pb^{2+}$  to Site 2 exceeds that of  $Ca^{2+}$  by 5- and 3-fold in the C2A and C2B domains, respectively.

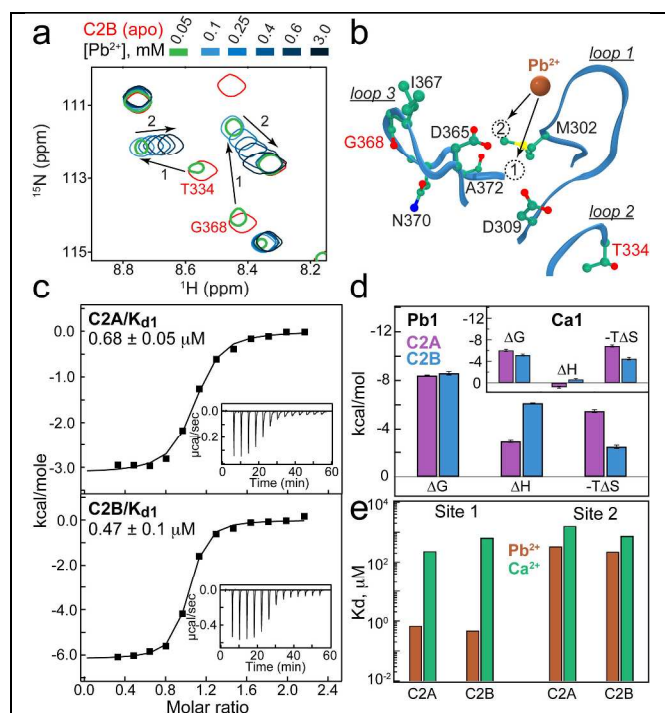


**Figure 3. C2 domains bind two  $Pb^{2+}$  ions in solution, with differential affinities.** (a) Expansions of C2B  $^{15}N$ - $^1H$  HSQC region for  $Pb^{2+}$  concentrations ranging from 0 to 3 mM. Peak displacements due to binding Pb1 (1, slow exchange) and Pb2 (2, fast exchange) are shown with arrows. (b) Loop region of C2B showing the location of  $Ca^{2+}$  sites 1 and 2 that are populated by  $Pb^{2+}$  in solution. (c) ITC profiles for Pb1 association with C2A (top) and C2B (bottom), and the respective dissociation constants. (d) Thermodynamic parameters of Pb1 binding to C2 domains. The inset shows Ca1 data reported in the previous study.<sup>45</sup> (e) Comparison of  $Pb^{2+}$  and  $Ca^{2+}$  affinities to sites 1 and 2 measured under identical conditions.

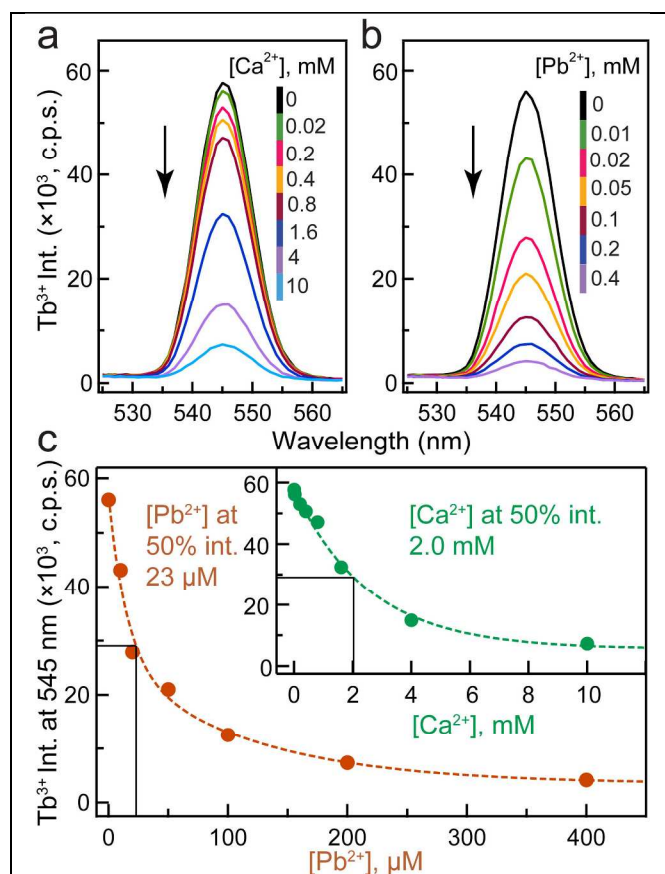
1  
2  
3 The slow exchange regime displayed by  $\text{Pb}^{2+}$  binding to Site 1 is generally unsuitable for the  
4 determination of binding affinities. We therefore conducted ITC experiments to obtain the  
5 dissociation constants ( $K_d$ ) and thermodynamic parameters of  $\text{Pb}^{2+}$  binding to Site 1. The  $K_d$   
6 values of Pb1 are in the sub-micromolar range for both domains:  $0.68 \pm 0.05 \mu\text{M}$  (C2A) and  $0.47$   
7  $\pm 0.1 \mu\text{M}$  (C2B), respectively (**Fig. 3c**). This represents 340-fold (C2A) and 1,400-fold (C2B)  
8 enhancement of  $\text{Pb}^{2+}$  affinities compared to those of  $\text{Ca}^{2+}$  under identical buffer conditions.<sup>31</sup>  
9  
10 The underlying thermodynamic basis of this enhancement is evident from the comparison of the  
11 enthalpic and entropic contributions to  $\Delta G$  (**Fig. 3d**). Pb1 binding to C2 domains is significantly  
12 exothermic. Combined with the favorable entropic contribution, this leads to large negative  $\Delta G$   
13 values. In contrast, the enthalpic contribution to Ca1 binding is small (inset of **Fig. 3d**), with  $\Delta G$   
14 being dominated by the entropy term. Therefore, it is mostly the differences in binding  
15 enthalpies that are responsible for the differential affinities of Pb1 and Ca1. The positive entropy  
16 change for both metal ions indicates that the gain due to metal de-solvation<sup>46</sup> is sufficient to  
17 compensate for the loss of conformational flexibility of metal ion-coordinating ligands.  
18  
19  
20  
21  
22  
23  
24  
25  
26  
27  
28  
29  
30  
31  
32  
33  
34  
35

36 A comparative summary of the binding data illustrates the two main conclusions of our  
37 experiments (**Fig. 3e**). First,  $\text{Pb}^{2+}$  populates Sites 1 and 2 in solution, with Pb1 affinity  
38 exceeding that of Pb2 by ~500-fold; this property enabled us to selectively probe  $\text{Pb}^{2+}$  binding  
39 events using ITC and NMR. Second,  $\text{Pb}^{2+}$  affinities are higher than those of  $\text{Ca}^{2+}$  for both C2  
40 domains. The enhancement of  $\text{Pb}^{2+}$  affinities compared to those of  $\text{Ca}^{2+}$  is significantly more  
41 pronounced for Site 1, which is the only site populated in the crystal structures of C2A and C2B.  
42  
43  
44  
45  
46  
47  
48  
49

50 Our conclusions regarding differential affinities of  $\text{Pb}^{2+}$  and  $\text{Ca}^{2+}$  to the C2 domains of SytI  
51 are further supported by the results of  $\text{Tb}^{3+}$  displacement experiments (**Fig. 4**).  $\text{Tb}^{3+}$  binds to the  
52 cytoplasmic region of SytI that contains both C2A and C2B domains (C2AB) with an apparent  
53  
54  
55  
56  
57  
58  
59  
60



1  
2  
3 affinity of 2.5  $\mu\text{M}$  (data not shown). When bound to C2AB,  $\text{Tb}^{3+}$  shows a strong luminescence  
4  
5 signal due to FRET from the tryptophan sidechains. We prepared a fully  $\text{Tb}^{3+}$ -saturated C2AB  
6  
7 and monitored the intensity changes of the strongest luminescence peak at 545 nm upon addition  
8  
9 of  $\text{Ca}^{2+}$  and  $\text{Pb}^{2+}$  (Fig. 4a,b). It takes  $\sim 100$ -fold more  $\text{Ca}^{2+}$  than  $\text{Pb}^{2+}$  to achieve  $\sim 50\%$   $\text{Tb}^{3+}$   
10  
11 displacement from C2AB (Fig. 4c), clearly indicating the thermodynamic preference for  $\text{Pb}^{2+}$   
12  
13 displacement from C2AB (Fig. 4c), clearly indicating the thermodynamic preference for  $\text{Pb}^{2+}$   
14  
15 over  $\text{Ca}^{2+}$ .



16  
17  
18  
19  
20  
21  
22  
23  
24  
25  
26  
27  
28  
29  
30  
31  
32  
33  
34  
35  
36  
37  
38  
39  
40  
41  
42  
43  
44  
45  
46  
47  
48  
49  
50  
51  
52  
53  
54  
55  
56  
57  
58  
59  
60

**Figure 4.  $\text{Pb}^{2+}$  is more potent than  $\text{Ca}^{2+}$  in displacing  $\text{Tb}^{3+}$  from the SytI C2AB region.** The most intense  $\text{Tb}^{3+}$  emission peak at 545 nm ( $^5\text{D}_4$  to  $^7\text{F}_5$  transition) is shown as a function of increasing  $\text{Ca}^{2+}$  (a) and  $\text{Pb}^{2+}$  (b) concentrations. The decrease in luminescence is indicative of the displacement of  $\text{Tb}^{3+}$  from the protein by  $\text{Ca}^{2+}$  and  $\text{Pb}^{2+}$ . (c) Intensity decrease at 545 nm plotted as a function of  $\text{M}^{2+}$  ( $\text{M}=\text{Ca}, \text{Pb}$ ).

1  
2  
3 It is well established that the affinities of divalent metal ions to C2 domains significantly  
4 increase in the vicinity of anionic lipids, in what Falke coined as a “target-activated messenger  
5 affinity” (TAMA) mechanism.<sup>47</sup> The implication is that intrinsic metal-ion affinities that we  
6 measure in solution are 2-3 orders of magnitude lower than those at the membrane surface. This  
7 mechanism provides an explanation of why C2 domains, being intrinsically weak  $\text{Ca}^{2+}$ -binding  
8 modules in solution, are able to respond to low micromolar  $\text{Ca}^{2+}$  concentrations during the cell-  
9 signaling event. In the framework of the TAMA mechanism, the affinity of  $\text{Pb}^{2+}$  to Site 1 would  
10 be comparable to the bioavailable concentration of  $\text{Pb}^{2+}$ , which ranges from picomolar to  
11 nanomolar.<sup>48</sup> This would make  $\text{Pb}^{2+}$  binding feasible under physiological conditions. The role  
12 of  $\text{Ca}^{2+}$  binding to Site 1 in C2 domains is the initial weak recruitment of the protein complex to  
13 the membranes, with the subsequent population of remaining  $\text{Ca}^{2+}$  site(s) to ensure high-affinity  
14 interaction.<sup>47</sup> Consistent with these findings, we observed very weak interactions between the  
15 C2·Pb1 complexes and phosphatidylserine-containing LUVs (data not shown), but almost full  
16 membrane association of C2 under saturating  $\text{Pb}^{2+}$  conditions (**Fig. S2**). Based on the above  
17 considerations, we conclude that: (i)  $\text{Pb}^{2+}$  is isofunctional to  $\text{Ca}^{2+}$  in its ability to support the C2-  
18 membrane interactions; and (ii) interactions of  $\text{Ca}^{2+}$  and  $\text{Pb}^{2+}$  with Site 1 of C2 domains will  
19 primarily determine the competitive behavior of these metal ions. We next sought to explore the  
20 properties of the C2·Pb1 complexes that – in addition to relative Ca1 and Pb1 affinities (**Fig. 3e**)  
21 – are most relevant for  $\text{Pb}^{2+}/\text{Ca}^{2+}$  competition: the kinetics of  $\text{Pb}^{2+}$  binding to Site 1 and the  
22 formation of mixed metal ion C2 species.

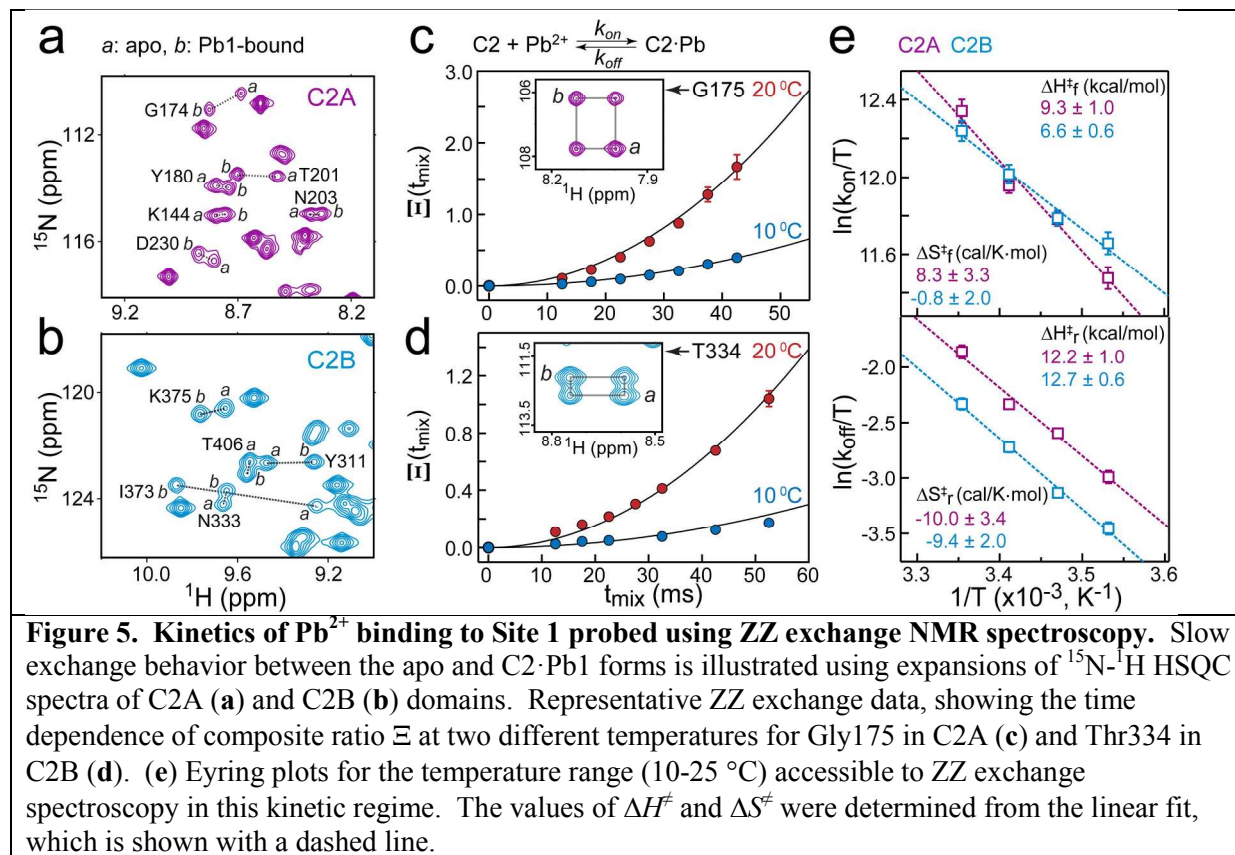
### 51 **Fast binding and slow dissociation of $\text{Pb}^{2+}$ from Site 1**

52  
53  
54  
55  
56  
57  
58  
59  
60

1  
2  
3 To obtain the kinetic information on  $\text{Pb}^{2+}$  binding to Site 1 of the C2A and C2B domains, we  
4 used the ZZ-exchange solution NMR spectroscopy. The method relies on the exchange of  
5 longitudinal magnetization between two C2 domain species: apo and single  $\text{Pb}^{2+}$ -bound, C2·Pb1  
6 (Fig. 5a,b). The inter-conversion between apo C2 and C2·Pb1 gives rise to cross-peaks (inset of  
7 Fig. 5c,d). The time-dependence of the auto- and cross-peak intensities, expressed through the  
8 composite ratio  $\Xi$ ,<sup>42</sup> contains information on the on- and off-rate constants for  $\text{Pb}^{2+}$  binding to  
9 Site 1 (Figs. S3-4 and Fig. 5c,d). The NMR data analysis produced the on-rate constants:  $(6.8 \pm$   
10  $0.4) \times 10^7 \text{ M}^{-1}\text{s}^{-1}$  (C2A) and  $(6.2 \pm 0.3) \times 10^7 \text{ M}^{-1}\text{s}^{-1}$  (C2B) that are close to the diffusion limit of  
11  $6 \times 10^8 \text{ M}^{-1}\text{s}^{-1}$  at 25 °C.<sup>49</sup> Moreover, the  $\text{Pb}^{2+}$   $k_{on}$  values are comparable to the  $k_{on}$  value  
12 previously reported for Ca1 binding to the C2A domain,  $(3.9 \pm 0.8) \times 10^7 \text{ M}^{-1}\text{s}^{-1}$ .<sup>50</sup> In contrast to  
13  $k_{on}$ , the  $\text{Pb}^{2+}$   $k_{off}$  values of 45.5 (C2A) and 29  $\text{s}^{-1}$  (C2B) are approximately two orders of  
14 magnitude smaller than the 2000-9500  $\text{s}^{-1}$  range previously reported for  $\text{Ca}^{2+}$ .<sup>50-52</sup> Therefore, the  
15 differential affinities of  $\text{Ca}^{2+}$  and  $\text{Pb}^{2+}$  to Site 1 are due to the differences in the off-rate  
16 constants.

17  
18  
19  
20  
21  
22  
23  
24  
25  
26  
27  
28  
29  
30  
31  
32  
33  
34  
35  
36 The temperature-dependent kinetics data were further used to estimate the activation  
37 enthalpy  $\Delta H^\ddagger$  and activation entropy  $\Delta S^\ddagger$  for the forward and reverse reactions (Fig. 5e).  
38 Although the enthalpic barrier  $\Delta H^\ddagger_f$  for the C2A- $\text{Pb}^{2+}$  association (9.3 kcal/mol) is larger than  
39 that of C2B (6.6 kcal/mol), the accompanying differences in  $\Delta S^\ddagger_f$  values produce essentially  
40 identical  $\Delta G^\ddagger_f$  values for C2A and C2B, 6.8 kcal/mol at 25 °C. This is only 1.8 kcal/mol larger  
41 than the theoretically predicted energy cost of ~5 kcal/mol required to transport a small molecule  
42 at the diffusion limit.<sup>49</sup> The negligible  $\Delta S^\ddagger_f$  for the C2B- $\text{Pb}^{2+}$  association indicates that the gain  
43 in solvent entropy due to de-solvation of  $\text{Pb}^{2+}$  and protein binding region is offset by a loss of  
44 conformational flexibility of C2B in the transition state. This is in contrast to C2A, where the  
45  
46  
47  
48  
49  
50  
51  
52  
53  
54  
55  
56  
57  
58  
59  
60

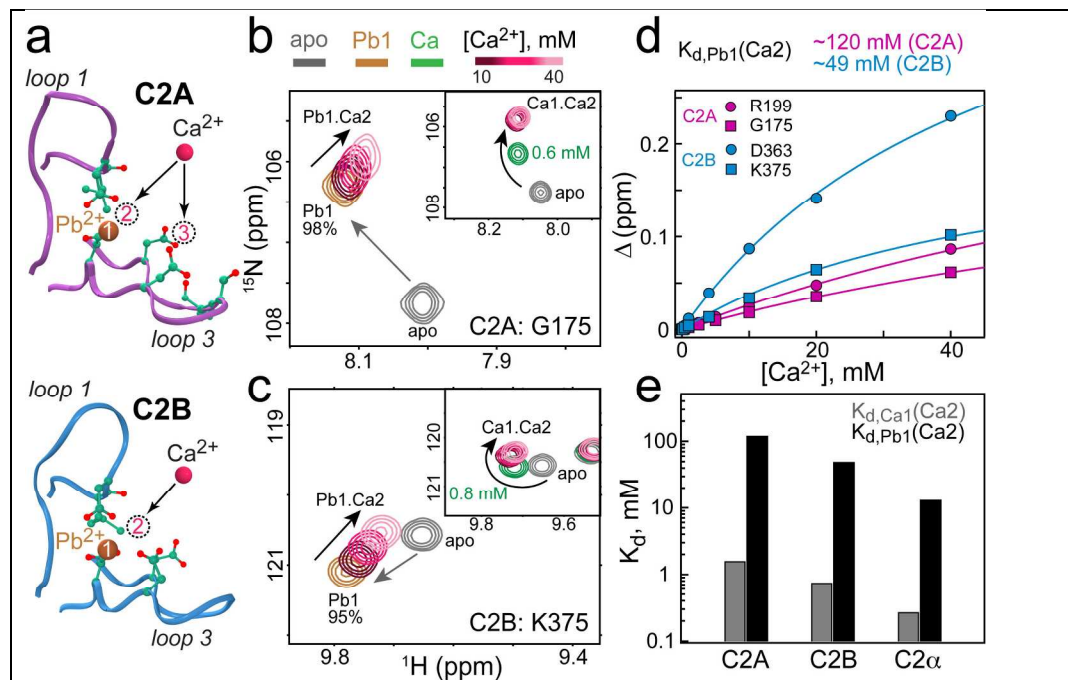
positive value of  $\Delta S^\ddagger_f$  suggests that conformational flexibility in the transition state is partially preserved. In the reverse (dissociation) direction, the activation parameters for the C2A and C2B are similar, with enthalpy and entropy terms contributing 80% and 20% to  $\Delta G^\ddagger_r$ , respectively. In aggregate, our data suggest that  $\text{Pb}^{2+}$  can act as both a thermodynamic and kinetic trap for the C2 domains and thereby effectively compete with  $\text{Ca}^{2+}$  for Site 1.



### $\text{Pb}^{2+}$ binding to Site 1 locks C2 domains in $\text{Ca}^{2+}$ -insensitive state

One potential mechanism through which  $\text{Ca}^{2+}$  can possibly rescue<sup>53</sup> the  $\text{Pb}^{2+}$ -induced protein behavior is through the formation of mixed metal ion species, with  $\text{Pb}^{2+}$  populating Site 1 and  $\text{Ca}^{2+}$  populating Site(s) 2 and 3, respectively (Fig. 6a). To test if this could be the case in SytI, we prepared C2·Pb1 complexes and evaluated their  $\text{Ca}^{2+}$ -binding behavior in the  $\text{Ca}^{2+}$  concentration range from 0.1 to 40 mM, using solution NMR spectroscopy. The NMR samples

were prepared such that the populations of C2A·Pb1 and C2B·Pb1 complexes were the dominant species ( $\geq 95\%$ ), with negligible population of Site 2 by  $\text{Pb}^{2+}$ . To our surprise, it took mM  $\text{Ca}^{2+}$  concentrations to detect noticeable shifts in the NMR spectra of C2·Pb1. Only at very high concentrations of  $\text{Ca}^{2+}$  (10-40 mM) did we observe a clear titratable  $\text{Ca}^{2+}$ -dependent behavior of cross-peaks that belong to the loop residues (**Fig. 6b,c; Fig S5**).



This is in sharp contrast with the  $\text{Ca}^{2+}$ -only binding data that showed full saturation of Sites 1 and 2 at  $\sim 10$  mM  $\text{Ca}^{2+}$  (insets of **Fig. 6b,c**). The dissociation constants of  $\text{Ca}^{2+}$  from Site 2 of the

1  
2  
3 C2A·Pb1 complexes,  $K_{d,Pb1}(Ca2)$ , obtained from the NMR data analysis are ~120 and ~49 mM  
4  
5 for the C2A and C2B, respectively (**Fig. 6d**). Comparison of the  $K_{d,Pb1}(Ca2)$  with previously  
6  
7 reported  $K_{d,Ca1}(Ca2)$  values<sup>31</sup> indicates that population of Site 1 by  $Pb^{2+}$  reduces  $Ca^{2+}$  affinities to  
8  
9 Site 2 by 60-70 fold. Moreover, the same pattern holds for the C2 domain from another protein,  
10  
11 Protein Kinase C $\alpha$ <sup>23</sup> (**Fig. 6e**). Therefore, for three C2 domains that share about ~40% pairwise  
12  
13 sequence identity we observed the same pattern: binding of  $Pb^{2+}$  to the high-affinity Site 1 on C2  
14  
15 domains reduces the  $Ca^{2+}$  affinity to the remaining vacant sites.  
16  
17  
18

19  
20 In view of the modest structural changes caused by  $Pb^{2+}$  binding to the C2 domain, the most  
21  
22 likely explanation of this behavior lies in the electronic properties of  $Pb^{2+}$  influencing  $Ca^{2+}$   
23  
24 affinity through the “bridging” ligands. Inspection of the  $Ca^{2+}$ -complexed structures of C2A and  
25  
26 C2B shows that in each domain there are two oxygen atoms that bridge metal ions in Sites 1 and  
27  
28 2: O $\delta$ 1(Asp172) and O $\delta$ 1(Asp232) in C2A, and O $\delta$ 1(Asp303) and O $\delta$ 1(Asp365) in C2B (**Fig.**  
29  
30 **S6a,b**).<sup>44, 54</sup>  $Pb^{2+}$  is a stronger Lewis acid than  $Ca^{2+}$ , which is manifested in its higher  
31  
32 electronegativity.<sup>55, 56</sup> This implies that Pb-O bonds have a more covalent character than Ca-O  
33  
34 bonds. A significant depletion of electron density of bridging ligands by  $Pb^{2+}$  at Site 1 would  
35  
36 reduce their electron-donating abilities and result in the attenuation of  $Ca^{2+}$  affinities to Site 2. If  
37  
38 we apply the same rationale to describe  $Ca^{2+}$  interactions with Site 3 of the C2A·Pb1 complex,  
39  
40 then  $Ca^{2+}$  affinity should not be significantly affected because metal ions in Sites 1 and 3 do not  
41  
42 share any oxygen ligands. Indeed, the  $K_{d,Pb1}(Ca3)$  of 26 mM (**Fig. S6,c**) determined using our  
43  
44 NMR data is not significantly different from the >10 mM estimate reported for the  $Ca^{2+}$ -only  
45  
46 system.<sup>30</sup> Another important outcome of  $Ca^{2+}$ -binding experiments is that we did not observe  
47  
48 any evidence of  $Pb^{2+}$  displacement from Site 1 even at > 250-fold  $Ca^{2+}$  excess, further confirming  
49  
50 our prediction that  $Pb^{2+}$  can effectively compete with  $Ca^{2+}$  for Site 1.  
51  
52  
53  
54  
55  
56  
57  
58  
59  
60

## CONCLUSIONS

We have characterized the structural, thermodynamic, and kinetic aspects of  $\text{Pb}^{2+}$  interactions with the C2 domains of SytI, a key regulator of the synaptic vesicle fusion and neurotransmitter release. We established that the  $\text{Ca}^{2+}$ -binding Site 1 of the C2 domains is the most likely target of  $\text{Pb}^{2+}$  due to high affinity of the interactions. The slow dissociation kinetics of  $\text{Pb}^{2+}$  will increase the lifetime of the protein- $\text{Pb}^{2+}$  complexes in the cell and thereby make  $\text{Pb}^{2+}$  a potent competitor of  $\text{Ca}^{2+}$ . The most unexpected outcome of our study – the loss of  $\text{Ca}^{2+}$  sensitivity of the C2 domains when  $\text{Pb}^{2+}$  populates only a single high-affinity site – suggests possible mechanisms through which  $\text{Pb}^{2+}$ , despite its low bioavailability, can disrupt the function of  $\text{Ca}^{2+}$ -dependent proteins. For instance, the inhibition of  $\text{Ca}^{2+}$ -dependent synchronous release of neurotransmitters<sup>57-64</sup> observed upon  $\text{Pb}^{2+}$  exposure could be attributed to the failure of  $\text{Pb}^{2+}$ -complexed SytI to sense elevated intracellular  $\text{Ca}^{2+}$  concentrations. In addition, the ability of  $\text{Pb}^{2+}$  to support the membrane interactions of SytI can explain the observed stimulatory effect of  $\text{Pb}^{2+}$  on  $\text{Ca}^{2+}$ -independent spontaneous release.<sup>57-64</sup> Previously, Bouton et al<sup>19</sup> demonstrated that  $\text{Pb}^{2+}$  is ~1000-fold more potent than  $\text{Ca}^{2+}$  in driving the membrane association of the cytoplasmic region containing both C2 domains of SytI. Combined with the results reported here, this offers an intriguing possibility that, in contrast to a full complement of  $\text{Ca}^{2+}$  ions, only one  $\text{Pb}^{2+}$  ion per C2 domain might be sufficient to drive the membrane interactions of SytI. Membrane-binding experiments on full-length SytI reconstituted into membrane-mimicking environment are required to address this question. Finally, our findings indicate that high-affinity interactions of  $\text{Pb}^{2+}$  with proteins are not limited to the thiol-rich coordination sites,<sup>65-69</sup> but can also occur in the

1  
2  
3 all-oxygen coordination environment provided by the C2 domains, the Ca<sup>2+</sup>-sensing membrane-  
4  
5 binding modules found in many signaling proteins.  
6  
7  
8  
9  
10  
11  
12  
13  
14  
15  
16  
17  
18  
19  
20  
21  
22  
23  
24  
25  
26  
27  
28  
29  
30  
31  
32  
33  
34  
35  
36  
37  
38  
39  
40  
41  
42  
43  
44  
45  
46  
47  
48  
49  
50  
51  
52  
53  
54  
55  
56  
57  
58  
59  
60



1  
2  
3 **Author Contributions:** T.I.I. and S.K. designed the study. T.I.I. directed the project. S.K.  
4 conducted the NMR spectroscopy, vesicle co-sedimentation, and luminescence experiments,  
5  
6 along with the corresponding data analysis. B.H. and A.K.S. contributed to sample preparation  
7  
8 and initial stages of the NMR and luminescence work. Samples for crystallization trials were  
9  
10 prepared by B.H., A.K.S. and S.K. Structure determination by X-Ray crystallography was  
11  
12 carried out by A.B.T. ITC data acquisition and processing were done by S.W.L. using protein  
13  
14 samples prepared by S.K. T.I.I. and S.K. wrote the manuscript with input from all authors.  
15  
16  
17  
18  
19  
20

21 **Acknowledgement:** This work was supported by the NSF CAREER Award CHE-1151435 to  
22  
23 T.I.I. A.K.S. and S.K. were supported by the NIH Grant R01GM108998 (T.I.I.) and Welch  
24  
25 Foundation Grant A-1784 (T.I.I.), respectively. The X-Ray Crystallography Core Laboratory is  
26  
27 supported by the Office of the Vice President for Research and by the NIH/NCI Grant P30  
28  
29 CA054174 award to the Mays Cancer Center, the newly named center home to UT Health San  
30  
31 Antonio MD Anderson Cancer Center. S.W.L acknowledges the support from Welch  
32  
33 Foundation grant A-1742.  
34  
35  
36  
37  
38  
39  
40  
41  
42  
43  
44  
45  
46  
47  
48  
49  
50  
51  
52  
53  
54  
55  
56  
57  
58  
59  
60

## REFERENCE

1. Y. C. Lo, C. A. Dooyema, A. Neri, J. Durant, T. Jefferies, A. Medina-Marino, L. de Ravello, D. Thoroughman, L. Davis, R. S. Dankoli, M. Y. Samson, L. M. Ibrahim, O. Okechukwu, N. T. Umar-Tsafe, A. H. Dama and M. J. Brown, Childhood lead poisoning associated with gold ore processing: a village-level investigation-Zamfara State, Nigeria, October-November 2010, *Environ. Health Perspect.*, 2012, **120**, 1450-1455.
2. M. Hanna-Attisha, J. LaChance, R. C. Sadler and A. Champney Schnepf, Elevated Blood Lead Levels in Children Associated With the Flint Drinking Water Crisis: A Spatial Analysis of Risk and Public Health Response, *Am. J. Public Health*, 2016, **106**, 283-290.
3. R. L. Canfield, C. R. Henderson Jr, D. A. Cory-Slechta, C. Cox, T. A. Jusko and B. P. Lanphear, Intellectual impairment in children with blood lead concentrations below 10 µg per deciliter, *N. Engl. J. Med.*, 2003, **348**, 1517-1526.
4. D. C. Bellinger, Very low lead exposures and children's neurodevelopment, *Curr. Opin. Pediatr.*, 2008, **20**, 172-177.
5. B. B. Gump, M. J. Dykas, J. A. MacKenzie, A. K. Dumas, B. Hruska, C. K. Ewart, P. J. Parsons, C. D. Palmer and K. Bendinskas, Background lead and mercury exposures: Psychological and behavioral problems in children, *Environ. Res.*, 2017, **158**, 576-582.
6. R. Deane and M. Bradbury, Transport of Lead - 203 at the Blood - Brain Barrier During Short Cerebrovascular Perfusion with Saline in the Rat, *J. Neurochem.*, 1990, **54**, 905-914.
7. H. A. Godwin, The biological chemistry of lead, *Curr. Opin. Chem. Biol.*, 2001, **5**, 223-227.
8. R. Gorkhali, K. Huang, M. Kirberger and J. J. Yang, Defining potential roles of Pb(2+) in neurotoxicity from a calciomics approach, *Metallomics*, 2016, **8**, 563-578.
9. M. Kirberger, Pb (II) Disruption of Synaptic Activity Through Ca (II)-and Zn (II)-binding Proteins, *Neurotransmitter*, 2017, **4**, 1-14.
10. J. G. Pounds, R. Wright, D. Morrison and D. A. Casciano, Effect of lead on calcium homeostasis in the isolated rat hepatocyte, *Toxicol. Appl. Pharmacol.*, 1982, **63**, 389-401.
11. J. P. Bressler and G. W. Goldstein, Mechanisms of lead neurotoxicity, *Biochem. Pharmacol.*, 1991, **41**, 479-484.
12. T. I. Lidsky and J. S. Schneider, Lead neurotoxicity in children: basic mechanisms and clinical correlates, *Brain*, 2003, **126**, 5-19.
13. S. Caito, B. A. Lopes Ana Carolina, M. B. Paoliello Monica and M. Aschner, *Journal*, 2017, **17**.
14. D. Busselberg, M. L. Evans, H. Rahmann and D. O. Carpenter, Lead and zinc block a voltage-activated calcium channel of Aplysia neurons, *J. Neurophysiol.*, 1991, **65**, 786-795.
15. S. Peng, R. K. Hajela and W. D. Atchison, Characteristics of block by Pb<sup>2+</sup> of function of human neuronal L-, N-, and R-type Ca<sup>2+</sup> channels transiently expressed in human embryonic kidney 293 cells, *Mol. Pharmacol.*, 2002, **62**, 1418-1430.
16. A. P. Neal and T. R. Guilarte, Molecular neurobiology of lead (Pb(2+)): effects on synaptic function, *Mol. Neurobiol.*, 2010, **42**, 151-160.
17. M. Alkondon, A. C. Costa, V. Radhakrishnan, R. S. Aronstam and E. X. Albuquerque, Selective blockade of NMDA-activated channel currents may be implicated in learning deficits caused by lead, *FEBS Lett.*, 1990, **261**, 124-130.

18. P. Gavazzo, I. Zanardi, I. Baranowska-Bosiacka and C. Marchetti, Molecular determinants of Pb<sup>2+</sup> interaction with NMDA receptor channels, *Neurochem. Int.*, 2008, **52**, 329-337.
19. C. M. Bouton, L. P. Frelin, C. E. Forde, H. Arnold Godwin and J. Pevsner, Synaptotagmin I is a molecular target for lead, *J. Neurochem.*, 2001, **76**, 1724-1735.
20. E. Habermann, K. Crowell and P. Janicki, Lead and other metals can substitute for Ca<sup>2+</sup> in calmodulin, *Arch. Toxicol.*, 1983, **54**, 61-70.
21. P. Kursula and V. Majava, A structural insight into lead neurotoxicity and calmodulin activation by heavy metals, *Acta Crystallogr. Sect. F Struct. Biol. Cryst. Commun.*, 2007, **63**, 653-656.
22. J. Markovac and G. W. Goldstein, Picomolar concentrations of lead stimulate brain protein kinase C, *Nature*, 1988, **334**, 71-73.
23. K. A. Morales, M. Lasagna, A. V. Gribenko, Y. Yoon, G. D. Reinhart, J. C. Lee, W. Cho, P. Li and T. I. Igumenova, Pb<sup>2+</sup> as modulator of protein-membrane interactions, *J. Am. Chem. Soc.*, 2011, **133**, 10599-10611.
24. A. Romero-Hernandez, N. Simorowski, E. Karakas and H. Furukawa, Molecular Basis for Subtype Specificity and High-Affinity Zinc Inhibition in the GluN1-GluN2A NMDA Receptor Amino-Terminal Domain, *Neuron*, 2016, **92**, 1324-1336.
25. L. Tang, T. M. Gamal El-Din, J. Payandeh, G. Q. Martinez, T. M. Heard, T. Scheuer, N. Zheng and W. A. Catterall, Structural basis for Ca<sup>2+</sup> selectivity of a voltage-gated calcium channel, *Nature*, 2014, **505**, 56-61.
26. M. C. van Severen, J. P. Piquemal and O. Parisel, Lead Substitution in Synaptotagmin: A Case Study, *The Journal of Physical Chemistry B*, 2010, **114**, 4005-4009.
27. M. Kirberger and J. J. Yang, Structural differences between Pb<sup>2+</sup>- and Ca<sup>2+</sup>-binding sites in proteins: implications with respect to toxicity, *J. Inorg. Biochem.*, 2008, **102**, 1901-1909.
28. M. Geppert, Y. Goda, R. E. Hammer, C. Li, T. W. Rosahl, C. F. Stevens and T. C. Sudhof, Synaptotagmin I: a major Ca<sup>2+</sup> sensor for transmitter release at a central synapse, *Cell*, 1994, **79**, 717-727.
29. I. Fernandez, D. Arac, J. Ubach, S. H. Gerber, O. Shin, Y. Gao, R. G. Anderson, T. C. Sudhof and J. Rizo, Three-dimensional structure of the synaptotagmin I C2B-domain: synaptotagmin I as a phospholipid binding machine, *Neuron*, 2001, **32**, 1057-1069.
30. R. Fernandez-Chacon, A. Konigstorfer, S. H. Gerber, J. Garcia, M. F. Matos, C. F. Stevens, N. Brose, J. Rizo, C. Rosenmund and T. C. Sudhof, Synaptotagmin I functions as a calcium regulator of release probability, *Nature*, 2001, **410**, 41-49.
31. S. Katti, S. B. Nyenhuis, B. Her, A. K. Srivastava, A. B. Taylor, P. J. Hart, D. S. Cafiso and T. I. Igumenova, Non-Native Metal Ion Reveals the Role of Electrostatics in Synaptotagmin I-Membrane Interactions, *Biochemistry*, 2017, **56**, 3283-3295.
32. X. Zhang, J. Rizo and T. C. Sudhof, Mechanism of phospholipid binding by the C2A-domain of synaptotagmin I, *Biochemistry*, 1998, **37**, 12395-12403.
33. J. Bai, P. Wang and E. R. Chapman, C2A activates a cryptic Ca(2+)-triggered membrane penetration activity within the C2B domain of synaptotagmin I, *Proc. Natl. Acad. Sci. U. S. A.*, 2002, **99**, 1665-1670.
34. X. Shao, C. Li, I. Fernandez, X. Zhang, T. C. Sudhof and J. Rizo, Synaptotagmin-syntaxin interaction: the C2 domain as a Ca<sup>2+</sup>-dependent electrostatic switch, *Neuron*, 1997, **18**, 133-142.

- 1  
2  
3 35. Z. P. Pang, O. H. Shin, A. C. Meyer, C. Rosenmund and T. C. Sudhof, A gain-of-  
4 function mutation in synaptotagmin-1 reveals a critical role of Ca<sup>2+</sup>-dependent soluble  
5 N-ethylmaleimide-sensitive factor attachment protein receptor complex binding in  
6 synaptic exocytosis, *J. Neurosci.*, 2006, **26**, 12556-12565.
- 7  
8 36. Q. Zhou, Y. Lai, T. Bacaj, M. Zhao, A. Y. Lyubimov, M. Uervirojnangkoorn, O. B.  
9 Zeldin, A. S. Brewster, N. K. Sauter, A. E. Cohen, S. M. Soltis, R. Alonso-Mori, M.  
10 Chollet, H. T. Lemke, R. A. Pfuetzner, U. B. Choi, W. I. Weis, J. Diao, T. C. Sudhof and  
11 A. T. Brunger, Architecture of the synaptotagmin-SNARE machinery for neuronal  
12 exocytosis, *Nature*, 2015, **525**, 62-67.
- 13  
14 37. K. A. Morales and T. I. Igumenova, Synergistic Effect of Pb<sup>2+</sup> and Phosphatidylinositol  
15 4, 5-Bisphosphate on C2 Domain–Membrane Interactions, *Biochemistry*, 2012, **51**, 3349-  
16 3360.
- 17  
18 38. E. F. Pettersen, T. D. Goddard, C. C. Huang, G. S. Couch, D. M. Greenblatt, E. C. Meng  
19 and T. E. Ferrin, UCSF Chimera--a visualization system for exploratory research and  
20 analysis, *J. Comput. Chem.*, 2004, **25**, 1605-1612.
- 21  
22 39. F. Delaglio, S. Grzesiek, G. W. Vuister, G. Zhu, J. Pfeifer and A. Bax, NMRPipe: a  
23 multidimensional spectral processing system based on UNIX pipes, *J. Biomol. NMR*,  
24 1995, **6**, 277-293.
- 25  
26 40. W. Lee, M. Tonelli and J. L. Markley, NMRFAM-SPARKY: enhanced software for  
27 biomolecular NMR spectroscopy, *Bioinformatics*, 2015, **31**, 1325-1327.
- 28  
29 41. N. A. Farrow, O. Zhang, J. D. Forman-Kay and L. E. Kay, A heteronuclear correlation  
30 experiment for simultaneous determination of <sup>15</sup>N longitudinal decay and chemical  
31 exchange rates of systems in slow equilibrium, *J. Biomol. NMR*, 1994, **4**, 727-734.
- 32  
33 42. V. Z. Miloushev, F. Bahna, C. Ciatto, G. Ahlsen, B. Honig, L. Shapiro and A. G. Palmer  
34 III, Dynamic properties of a type II cadherin adhesive domain: implications for the  
35 mechanism of strand-swapping of classical cadherins, *Structure*, 2008, **16**, 1195-1205.
- 36  
37 43. L. Shimoni-Livny, J. P. Glusker and C. W. Bock, Lone Pair Functionality in Divalent  
38 Lead Compounds, *Inorg. Chem.*, 1998, **37**, 1853-1867.
- 39  
40 44. X. Shao, I. Fernandez, T. C. Sudhof and J. Rizo, Solution structures of the Ca<sup>2+</sup>-free and  
41 Ca<sup>2+</sup>-bound C2A domain of synaptotagmin I: does Ca<sup>2+</sup> induce a conformational  
42 change?, *Biochemistry*, 1998, **37**, 16106-16115.
- 43  
44 45. C. S. Evans, Z. He, H. Bai, X. Lou, P. Jeggle, R. B. Sutton, J. M. Edwardson and E. R.  
45 Chapman, Functional analysis of the interface between the tandem C2 domains of  
46 synaptotagmin-1, *Mol. Biol. Cell*, 2016, **27**, 979-989.
- 47  
48 46. J. L. Gifford, M. P. Walsh and H. J. Vogel, Structures and metal-ion-binding properties  
49 of the Ca<sup>2+</sup>-binding helix–loop–helix EF-hand motifs, *Biochem. J.*, 2007, **405**, 199-221.
- 50  
51 47. J. A. Corbin, J. H. Evans, K. E. Landgraf and J. J. Falke, Mechanism of specific  
52 membrane targeting by C2 domains: localized pools of target lipids enhance Ca<sup>2+</sup>  
53 affinity, *Biochemistry*, 2007, **46**, 4322-4336.
- 54  
55 48. E. S. Claudio, H. A. Godwin and J. S. Magyar, in *Prog. Inorg. Chem.*, John Wiley &  
56 Sons, Inc., 2003, DOI: 10.1002/0471267287.ch1, pp. 1-144.
- 57  
58 49. K. van Holde, A hypothesis concerning diffusion-limited protein–ligand interactions,  
59 *Biophys. Chem.*, 2002, **101**, 249-254.
- 60  
61 50. O. Millet, P. Bernado, J. Garcia, J. Rizo and M. Pons, NMR measurement of the off rate  
62 from the first calcium-binding site of the synaptotagmin I C2A domain, *FEBS Lett.*,  
63 2002, **516**, 93-96.

- 1
- 2
- 3
- 4 51. J. H. Bollmann, B. Sakmann and J. G. Borst, Calcium sensitivity of glutamate release in a
- 5 calyx-type terminal, *Science*, 2000, **289**, 953-957.
- 6 52. R. Schneggenburger and E. Neher, Intracellular calcium dependence of transmitter
- 7 release rates at a fast central synapse, *Nature*, 2000, **406**, 889-893.
- 8 53. X. Sun, X. Tian, J. L. Tomsig and J. B. Suszkiw, Analysis of differential effects of Pb<sup>2+</sup>
- 9 on protein kinase C isozymes, *Toxicol. Appl. Pharmacol.*, 1999, **156**, 40-45.
- 10 54. Y. Cheng, S. M. Sequeira, L. Malinina, V. Tereshko, T. H. Sollner and D. J. Patel,
- 11 Crystallographic identification of Ca<sup>2+</sup> and Sr<sup>2+</sup> coordination sites in synaptotagmin I
- 12 C2B domain, *Protein Sci.*, 2004, **13**, 2665-2672.
- 13 55. C. Cárdenas and P. W. Ayers, How reliable is the hard-soft acid-base principle? An
- 14 assessment from numerical simulations of electron transfer energies, *Phys. Chem. Chem.*
- 15 *Phys.*, 2013, **15**, 13959-13968.
- 16 56. K. Li, M. Li and D. Xue, Solution-phase electronegativity scale: Insight into the chemical
- 17 behaviors of metal ions in solution, *The Journal of Physical Chemistry A*, 2012, **116**,
- 18 4192-4198.
- 19 57. R. S. Manalis and G. P. Cooper, Letter: Presynaptic and postsynaptic effects of lead at the
- 20 frog neuromuscular junction, *Nature*, 1973, **243**, 354-356.
- 21 58. P. T. Carroll, E. K. Silbergeld and A. M. Goldberg, Alteration of central cholinergic
- 22 function by chronic lead acetate exposure, *Biochem. Pharmacol.*, 1977, **26**, 397-402.
- 23 59. D. J. Minnema, R. D. Greenland and I. A. Michaelson, Effect of in vitro inorganic lead
- 24 on dopamine release from superfused rat striatal synaptosomes, *Toxicol. Appl.*
- 25 *Pharmacol.*, 1986, **84**, 400-411.
- 26 60. D. J. Minnema, I. A. Michaelson and G. P. Cooper, Calcium efflux and neurotransmitter
- 27 release from rat hippocampal synaptosomes exposed to lead, *Toxicol. Appl. Pharmacol.*,
- 28 1988, **92**, 351-357.
- 29 61. S. M. Lasley and M. E. Gilbert, Presynaptic glutamatergic function in dentate gyrus in
- 30 vivo is diminished by chronic exposure to inorganic lead, *Brain Res.*, 1996, **736**, 125-
- 31 134.
- 32 62. L. Struzynska and U. Rafalowska, The effect of lead on dopamine, GABA and histidine
- 33 spontaneous and KCl-dependent releases from rat brain synaptosomes, *Acta Neurobiol.*
- 34 *Exp. (Wars.)*, 1994, **54**, 201-207.
- 35 63. M. T. Antonio and M. L. Leret, Study of the neurochemical alterations produced in
- 36 discrete brain areas by perinatal low-level lead exposure, *Life Sci.*, 2000, **67**, 635-642.
- 37 64. S. M. Lasley and M. E. Gilbert, Rat hippocampal glutamate and GABA release exhibit
- 38 biphasic effects as a function of chronic lead exposure level, *Toxicol. Sci.*, 2002, **66**, 139-
- 39 147.
- 40 65. T. J. Simons, The affinity of human erythrocyte porphobilinogen synthase for Zn<sup>2+</sup> and
- 41 Pb<sup>2+</sup>, *Eur. J. Biochem.*, 1995, **234**, 178-183.
- 42 66. P. T. Erskine, N. Senior, S. Awan, R. Lambert, G. Lewis, I. J. Tickle, M. Sarwar, P.
- 43 Spencer, P. Thomas, M. J. Warren, P. M. Shoolingin-Jordan, S. P. Wood and J. B.
- 44 Cooper, X-ray structure of 5-aminolaevulinatase dehydratase, a hybrid aldolase, *Nat.*
- 45 *Struct. Biol.*, 1997, **4**, 1025-1031.
- 46 67. J. S. Magyar, T. C. Weng, C. M. Stern, D. F. Dye, B. W. Rous, J. C. Payne, B. M.
- 47 Bridgewater, A. Mijovilovich, G. Parkin, J. M. Zaleski, J. E. Penner-Hahn and H. A.
- 48 Godwin, Reexamination of lead(II) coordination preferences in sulfur-rich sites:
- 49
- 50
- 51
- 52
- 53
- 54
- 55
- 56
- 57
- 58
- 59
- 60

- 1  
2  
3 implications for a critical mechanism of lead poisoning, *J. Am. Chem. Soc.*, 2005, **127**,  
4 9495-9505.  
5  
6 68. K. P. Neupane and V. L. Pecoraro, Probing a homoleptic PbS3 coordination environment  
7 in a designed peptide using <sup>207</sup>Pb NMR spectroscopy: implications for understanding the  
8 molecular basis of lead toxicity, *Angew. Chem. Int. Ed. Engl.*, 2010, **49**, 8177-8180.  
9  
10 69. J. M. Ordemann and R. N. Austin, Lead neurotoxicity: exploring the potential impact of  
11 lead substitution in zinc-finger proteins on mental health, *Metalloomics*, 2016, **8**, 579-588.  
12  
13  
14  
15  
16  
17  
18  
19  
20  
21  
22  
23  
24  
25  
26  
27  
28  
29  
30  
31  
32  
33  
34  
35  
36  
37  
38  
39  
40  
41  
42  
43  
44  
45  
46  
47  
48  
49  
50  
51  
52  
53  
54  
55  
56  
57  
58  
59  
60